UWB on-body radio propagation and system modelling for wireless body-centric networks

A. Alomainy, Y. Hao, X. Hu, C.G. Parini and P.S. Hall

Abstract: Given the trend towards a user-centric concept in mobile communications, body area networks have received increasing attention within the wireless personal area community. Researchers and designers have been investigating radio propagation characterisation and modelling owing to its importance in developing and designing efficient and reliable radio systems. The paper presents an experimental investigation of ultra-wideband (UWB) on-body radio propagation. Channel models with respect to large scale and delay analysis have been derived from measured parameters. Effects of different antenna types on channel behaviour are also demonstrated. Results and analyses highlight the consequences of changes in body postures and positions in addition to antenna orientations on the communication channels. Measurement data are also used in predicting the performance of potential UWB wireless systems and their applications in body-centric networks. It is indicated that bi-phase modulation for UWB body-centric networks performs better than pulse position modulation systems. The study also concludes that the use of hybrid antenna types for different on-body links will provide better system performance.

1 Introduction

Future communication systems are driven by the concept of being connected anywhere at anytime. An essential part of this concept is a user-centric approach in which services are constantly available and systems provide re-configurability, unobtrusiveness and true extension of the human mind. Body-centric networks consist of a number of nodes and units placed on the human body or in close proximity such as on everyday clothing [1]. Since low-power transmission is required for body worn wireless devices, the human body can be used as a communication channel between wireless wearable devices to form a wireless body-centric network.

Ultra-wideband (UWB) communication is a low-power, high data rate technology with large bandwidth signals that provide robustness to jamming and have low probability of detection [2]. UWB low transmit power requirements allow longer battery life for body worn units. This leads to UWB being a potential candidate for body-centric networks. UWB offers good penetrating properties that could be applied to imaging in medical applications; with the UWB body sensors, this application could be easily reconfigured to adapt to the specific tasks and would enable high data rate connectivity to external processing networks.

The wireless body-centric network has special properties and requirements in comparison to other available wireless networks and that is due to the rapid changes in communication channel behaviour on the body during the network operation. This raises some important issues regarding the propagation channel characteristics, radio systems compatibility with such environments and the effect that it has on the wearer. In the last few years, researchers have investigated UWB indoor and outdoor radio propagation modelling and characterisation [3, 4]. However, on-body channel characterisation has been presented in few studies [5, 6] for narrowband channels. UWB body area network channel characterisation was presented in [7] only for pre-defined sets of nodes with multi-hopping networking in mind to determine energy and power requirements, whereas more realistic representation of human body behaviour such as different body positions and the effects of various antenna types on UWB on-body channels was investigated in [8]. The performance of UWB radio systems in multipath indoor environment has been presented in [9, 10]. However, to the authors' knowledge, system-level modelling of potential on-body UWB radio systems with measured channel data and delay profile modelling has not been presented.

In this paper, we demonstrate an experimental investigation of UWB on-body radio channels through a measurement campaign performed in order to obtain sufficient path variation data for effective characterisation of the channels. Two types of UWB antennas were used to examine on-body propagation inside an anechoic chamber. Path loss models and spread delay behaviour in comparison to established propagation models are also presented. Such measurements could provide deterministic characterisations that can be applied in designing simple and efficient body-centric radio systems. A system-level modelling of a possible UWB RF transceiver, based on pulse position modulation (PPM) and bi-phase modulation with measured channel parameters, is also demonstrated.

IEE Proceedings online no. 20050046

doi:10.1049/ip-com:20050046

Paper first received 31st January and in final revised form 12th July 2005

A. Alomainy, Y. Hao, X. Hu and C.G. Parini are with Department of Electronic Engineering, Queen Mary, University of London London, E1 4NS, UK

P.S. Hall is with School of Electronic, Electrical and Computer Engineering, University of Birmingham, Birmingham B15 2TT, UK

E-mail: y.hao@elec.qmul.ac.uk

2 UWB on-body propagation channel characterisation

2.1 Frequency domain measurement setup

A Hewlett Packard 8720ES vector network analyser (VNA) was set on the response mode in the range 3 GHz–9 GHz with intervals of 3.75 MHz, at a sweep rate of 800 ms, for UWB on-body communication channels measurement. Port-I was used as a transmit node and port-II as the receiver with two pairs of different UWB antennas to measure channel frequency response (S_{21}). Antennas were connected to the VNA by 3 and 5 metre long cables. The VNA measures the magnitude and phase of each frequency components allowing the ease of obtaining time domain response by means of inverse discrete fourier transform (IDFT). Two sets of measurements were performed in the anechoic chamber to account for deterministic channel characteristics on human body (height 170 cm and average width of 35 cm), which resulted in 710 frequency responses for different on-body channels. Figure 1 shows the different antenna positions placed on the body and the measurement setup. Twenty-two different on-body scenarios applied in the measurement, illustrating possible body movements and potential positions on body for worn devices, are listed in Table 1. The minimum measured distance is 15 cm, which is larger than the wavelength (10 cm) of the low frequency limit in the band (3 GHz), minimising the mutual coupling effect when antennas are placed near each other. Fifteen frequency sweeps were taken for each static on-body channel [8]. All measurements in this study were taken using effective isotropic radiated power (EIRP) of the order of 0 dBm, approximately 30 dB less than that emitted by cellular phones.

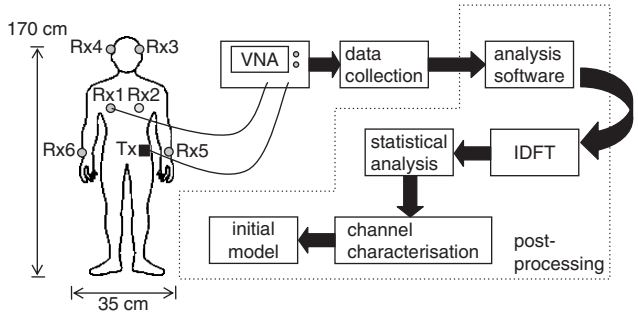

Fig. 1 *Antenna positions for on-body channel characterisation campaign with human body dimensions and measurement setup including post-processing steps*

2.2 Measured UWB antennas

Two pairs of UWB antennas (horn shaped self-complementary-HSCA, and planar inverted cone antenna-PICA) were designed following the descriptions outlined in [11] and [12]. The planar HSCA was fabricated on a RT/Duroid substrate with relative permittivity of 3 and thickness of 1.524 mm and overall dimensions of 100×100 mm (Fig. 2*a*). A 3-stage Chebyshev transformer backed with a 29.8×11.4 mm ground plated on the opposite side of the printed radiating elements is used to provide wideband matching to the 50 Ω coaxial cable feed. The HSCA exhibits approximately constant impedance and absolute gain across the UWB band with measured gain of 0 to 2.4 dBi. The second type of UWB antenna applied in the on-body propagation measurement is the PICA antenna, which is derived from the volcano antenna and the circular disk antenna concepts, Fig. 2*b*. It is composed of a single flat element vertically mounted above a small circular ground plane with a diameter of 60 mm. The antenna geometry is very simple with antenna dimensions of 29.2×76.2 mm and conductor thickness for the cone around 0.3 mm. The antenna provides outstanding impedance and radiation pattern performance with a gain of 3 to 6 dBi.

The impedance bandwidth performance of the two antennas is compared to UWB requirements. Impedance bandwidths of 10:1 and 8:1 were obtained for the HSCA and PICA antennas, respectively [8]. However, comparing the far field radiation patterns for both the azimuth plane (Fig. 3*a*, xz-plane co-polarisation) and elevation plane (Fig. 3*b*, yz-plane co-polarisation) of the two antennas at 3 and 10 GHz shows better radiation bandwidth obtained for the PICA case compared to HSCA. This leads to the fact that PICA has a better effective bandwidth across the UWB band of interest (3–9 GHz). Figure 3 illustrates the effect of the restriction on board size and addition of ground plane on the radiation performance of the HSCA at higher frequencies. Phase distortion caused by slight mismatching at these frequencies in the transformer circuit causes changes in transmission responses and also radiation pattern with the appearance of nulls obviously illustrated in Fig. 3 for the HSCA case. Detailed characterisation of both antennas is presented in [5, 6, 8].

The HSCA (planar dipole-like antenna) and PICA (vertical monopole-like antenna) antennas were chosen for

Table 1: Different 22 body scenarios and positions for UWB on-body measurement with related RMS spread delay statistics (RMS values and mean RMS)

N	On-body scenario	HSCA τ_{rms}	Mean RMS	PICA τ_{rms}	Mean RMS	N	On-body scenario	HSCA τ_{rms}	Mean RMS	PICA τ_{rms}	Mean RMS
1	Rx1 - standing still, upright	3.1		2.6		12	Rx4 - standing upright	3.7		3.7	
2	Rx1 - body turned left	3.4		2.9		13	Rx4 - head turned left	2.4	3.80	2	3.36
3	Rx1 - body turned right	1.9	2.47	2.2	2.74	14	Rx4 - head turned right	5.3		4.39	
4	Rx1 - body leaned forward	1.49		3.27		15	Rx5 - standing arm stretched	1.32		1.8	
5	Rx2 - (back) standing upright	10.7		7.65		16	Rx5 - standing arm above head	4	1.73	2.5	1.87
6	Rx2 - (back) body turned left	4.5	6.20	12.3	6.67	17	Rx5 - sitting arm along body	0.55		1.67	
7	Rx2 - (back) body turned right	3.98		2.97		18	Rx5 - sitting hand on lap	1.03		1.5	
8	Rx2 - (back) body leaned forward	5.6		3.74		19	Rx6 - standing arm stretched	3.4		3.7	
9	Rx3 - standing upright	1.23		1.25		20	Rx6 - standing arm above head	7.7	3.84	4.25	3.19
10	Rx3 - head turned left	4.5	2.91	2.6	1.91	21	Rx6 - sitting arm along body	3.2		2.8	
11	Rx3 - head turned right	3		1.87		22	Rx6 - sitting hand on lap	1.07		2	

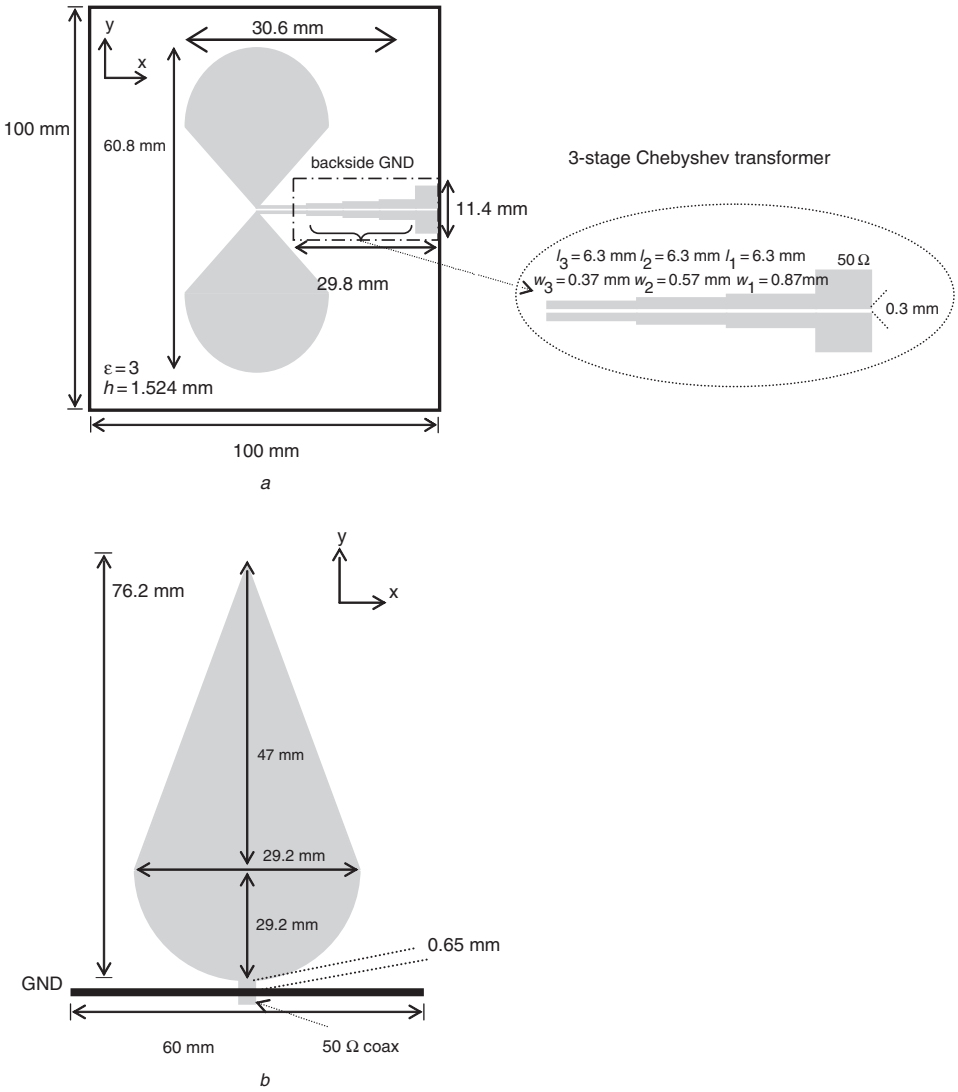

Fig. 2 *Detailed schematic diagrams of applied UWB antennas with dimensions in mm*
a Horn shaped self-complementary antenna (HSCA), placed parallel to the body with radiating element facing outwards from the body
b Planar inverted cone antenna (PICA), placed perpendicular to the body with ground plate on the body

the reported measurement campaign to provide a clear picture of the influence of antenna characteristics on propagation channel behaviour. Different antenna types are expected to have dissimilar effects on the radio channels especially in the body area network where the transmitter and the receiver are in close proximity. Hence, antenna near field characterisation is needed. Figures 4*a* and *b* show numerically computed near field patterns at a distance of 15 cm from the antenna in azimuth and elevation planes, respectively. In the measurement campaign, HSCA was placed parallel to the body with main radiating elements facing outward from the body. PICA was placed with the radiator perpendicular and the ground plate parallel to the body.

2.3 Data analysis

The measured channel data for different on-body scenarios were calculated and processed in both frequency and time domain (the setup shown in Fig. 1) to obtain initial statistical models for both path losses and power delay profiles including spread mean excess delay. Their reliability and applicability are investigated against established empirical and theoretical propagation models.

The average received power (S_{21}) is shown in Figs. 5*a* and *c* for scenario 15 when Rx5 is placed on the left wrist and the arm stretched aside the body and scenario 12 when Rx4 is placed on the right side of the head with head still facing forward (Table 1), respectively. Examining the slopes of these frequency responses shows the variation in slope values not only owing to antenna frequency dependency but also the dispersion of on-body channels.

Time domain analysis is performed by obtaining channel impulse responses that are calculated from the measured frequency transfer functions consisting of 1601 frequency points using the real passband technique and applying a Hamming window and inverse discrete fourier transform (IDFT) [3]. Time domain pulses for different sweeps were used to verify that channels were static during measurements for the specified on-body link in addition to verification in frequency domain [8]. Figures 5*b* and *d* present impulse responses for on-body scenario 15 and scenario 12 (as defined in Table 1). It can be seen that most energy is received via the direct path with some multipath reflections at the late time. The changes in channel characteristics owing to different antenna (HSCA and PICA) properties can be also found in these Figures. The main dissimilarity is that more strong echoes and ringing effects appear in the PICA case. This can be explained by the fact that the PICA has a narrower bandwidth and more resonance frequencies within the measured band, which

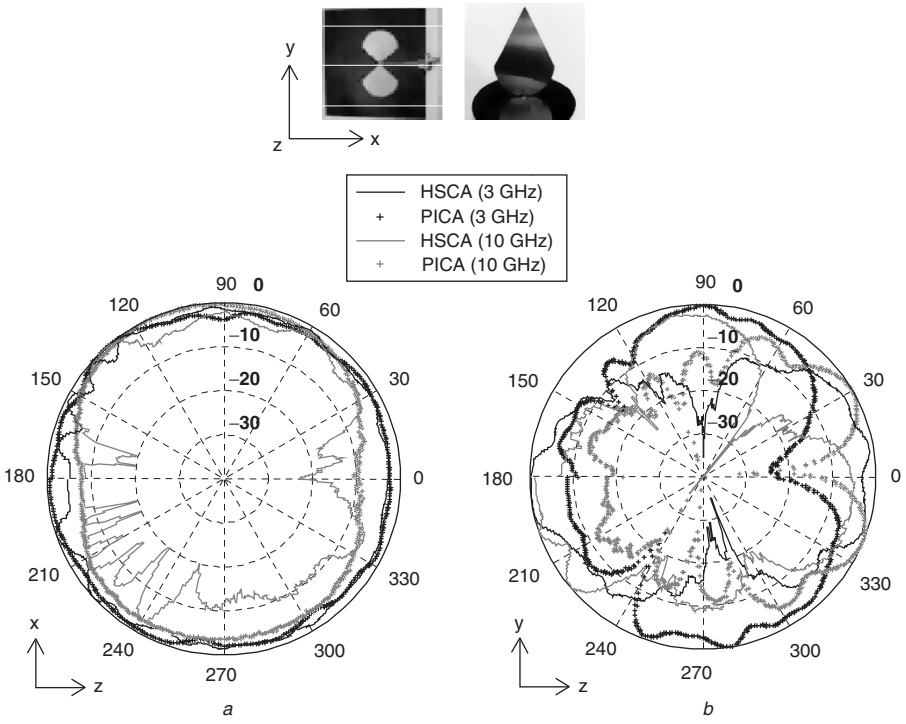

Fig. 3 *Comparison between measured HSCA and PICA far field radiation patterns at 3 GHz and 10 GHz Inset: Picture defines the antenna coordinates*
a Azimuth plane (xz-plane co-polarisation)
b Elevation plane (yz-plane co-polarisation)

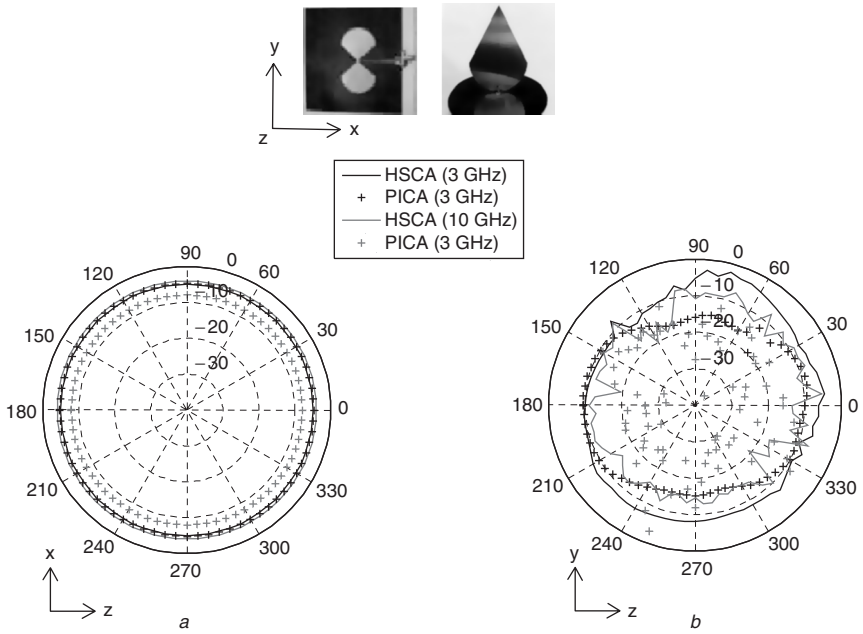

Fig. 4 *Comparison between computed near field patterns for HSCA and PICA at 3 and 10 GHz at 15 cm distance from the antenna*
Inset: Picture defines the antenna coordinates
a Azimuth plane (xz-plane E-total)
b Elevation plane (yz-plane E-total)

increases both the ringing and pulse width that directly affects data rate.

Power delay profiles (PDP) were produced by averaging all impulse responses and determining the noise threshold. The PDP is characterised by the first central moment (mean excess delay τ_m) and the square root of the second moment of the PDP (RMS delay spread τ_{rms}). The RMS delay spread provides a figure of merit for estimating data rates for multipath channels [13]. The mean excess delay is defined as

$$\tau_m = \sqrt{\frac{\sum_{i=0}^{N-1} \tau_i \cdot |h(\tau_i)|^2}{\sum_{i=0}^{N-1} |h(\tau_i)|^2}} \quad (1)$$

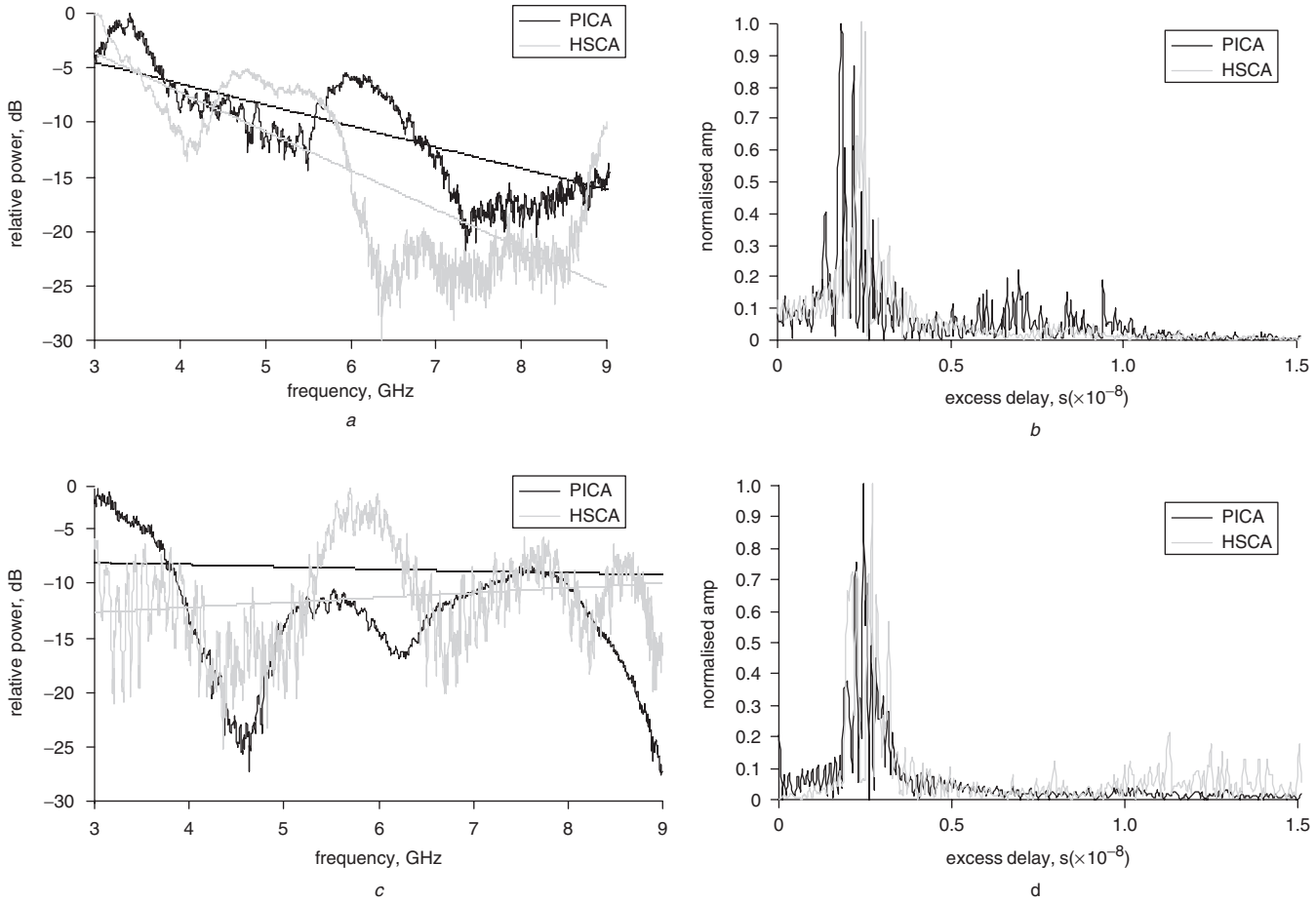

Fig. 5 *Measured channel frequency responses and impulse responses for on-body scenario 12 (Rx4-receiver on the right side of the head with body standing still) and scenario 15 (Rx5-receiver on the left wrist with arm stretched aside)*
a Channel frequency response scenario 15
b Impulse response scenario 15
c Channel frequency response scenario 12
d Impulse response scenario 12

and the delay spread τ_{rms} as

$$\tau_{rms} = \sqrt{\frac{\sum_{i=0}^{N-1} (\tau_i - \tau_m)^2 \cdot |h(\tau_i)|^2}{\sum_{i=0}^{N-1} |h(\tau_i)|^2}} \qquad (2)$$

where $h(\tau_i)$ is the time domain impulse response obtained from measurement data.

Delay parameters were evaluated for interval of 80 ns, since echoes fade rapidly after this period. Table 1 shows a summary of the RMS delay spread and mean RMS for both measurement sets (PICA and HSCA) for various on-body propagation scenarios. As expected, the mean delay owing to propagation link between the transmitter (Tx) and the receiver at the back (Rx2), Fig. 1, for scenarios 5, 6, 7 and 8 (Table 1) link is the highest where non-line-of-sight (NLOS) channel and propagation around human body on the surface (creeping waves) are the main propagation channels. Mean RMS delay for links with small distances and where both antennas are placed on the same part of the human body in the HSCA antenna case is smaller than RMS spread delay for the same links with PICA (cases Rx1, Rx2, Rx5). This can be related to the placement of both antennas of which stronger surface waves are launched in the HSCA case. For other links where line-of-sight (LOS) components (free space waves) are dominant, PICA produces better delay performance. Figure 6 shows the RMS delay spread against distance for both measurement cases while Figs. 7*a* and *b* show the cumulative distributions of the RMS delay spread and mean excess delay, respectively, fit to log normal distribution. Other different empirical distributions were applied, however, log normal proved to be the best fit with more deviation for PICA channels, which is predictable owing to the random behaviour of the on-body channels that could lead to a modified fit model for more extensive links.

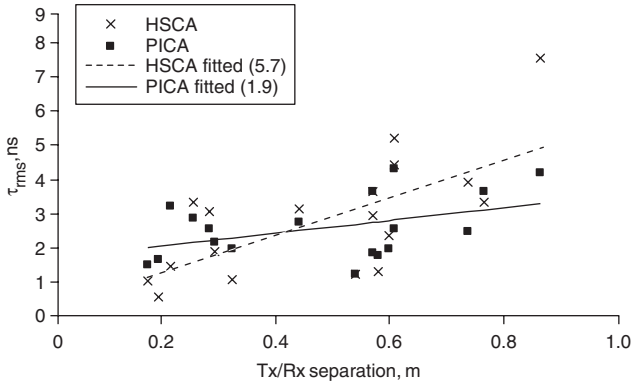

Fig. 6 *RMS delay spread variation against distance for both HSCA and PICA*

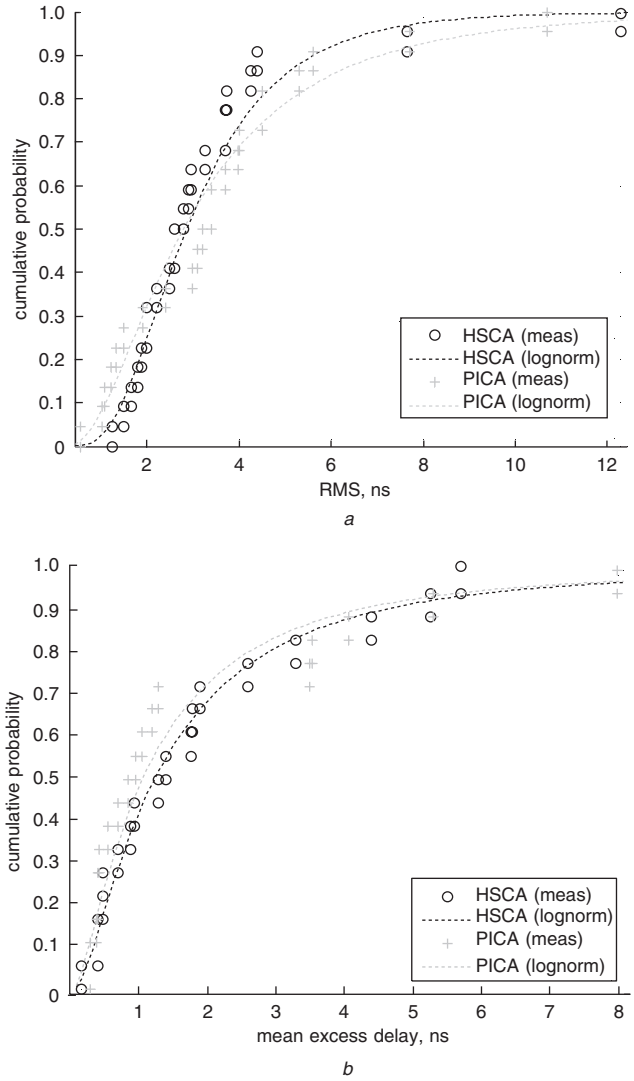

Fig. 7 *Delay parameters cumulative distribution fit to log normal distribution*
a RMS delay spread for on-body channels (τ_{rms})
b Mean excess delay (τ_m)

The path loss of the channel is calculated directly from the measurement data using averaging over the measured channel frequency responses at each frequency point [4]. The mean path loss referenced to a distance d_o (reference distance is 1 m as calibrated for VNA measurement) can be presented as a fitted line model for both cases.

For HSCA

$$PL_{dB}(d) = 86.5 + (4.4)10\log\left(\frac{d}{d_o}\right) \quad \text{for } 15\,\text{cm} \le d \le 100\,\text{cm} \tag{3}$$

and for PICA

$$PL_{dB}(d) = 70.3 + (2.7)10\log\left(\frac{d}{d_o}\right) \quad \text{for } 15\,\text{cm} \le d \le 100\,\text{cm} \tag{4}$$

where $\alpha = 4.4$ and 2.7 are the path loss exponents for HSCA and PICA models, respectively. Figure 8 presents the measured values and modelled path losses against distance for both antenna cases. It can be concluded from Fig. 8 that on-body channel path losses can be approximated using the conventional dual-slope model. It can be calculated that at the UWB band, the far field will be at

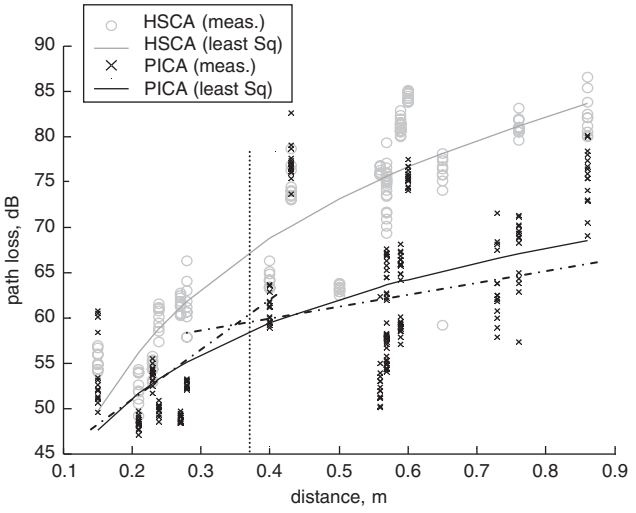

Fig. 8 *Measured and modelled path loss for HSCA and PICA with proposed dual-slope model for PICA case*

distances equal to and greater than 37 cm for PICA, which agrees with that from the measurement in Fig. 8 with a breakpoint around 37 cm.

The non-reflecting environment in the anechoic chamber leads to the high exponent of path losses, however, for PICA, good omni-directional radiation across UWB range results in the lower loss exponent value owing to multipath reflections from human body and clothes. In addition to distance changes and different body positions contribution to channel path loss, another important factor is antenna orientation considering both transmit and receive antennas. For example, an additional 20 dB loss will occur when two PICAs are orthogonally oriented on the body.

3 UWB radio system performance in a body-centric environment

3.1 System-level modelling

The wireless transceiver systems used in body-centric networks have to be ideally miniaturised, lightweight, exhibit low-power operation for longer lifetime and be easily integrated with daily clothing. The different parts in the system need to share a common wireless protocol to enable the establishment of a re-configurable communication medium. Sufficient data rates and controlled power levels are required by the radio transceivers to enable flawless connectivity between body-distributed networks. Many currently existing short-range wireless technologies provide communication medium and cable replacement technologies for different transmission types. To design a suitable efficient radio interface for the wireless body-centric network, the understanding and integration of existing standards are required in order to bring to light the main areas in which new techniques are required to meet the harsh and demanding communication environment.

The UWB radio front-end could be used for the same applications targeted for other short-range wireless systems, however, at higher data rates, lower emitted radio frequency (RF) power and less complexity in transceiver designs. Since accurate performance prediction of UWB systems requires the knowledge of the propagation channel behaviour, system modelling of potential UWB radio transceivers for body-centric network is proposed. Figure 9 shows a block diagram of the radio system modelled using Agilent DSP Designer™ to investigate the effects of on-body channels on UWB systems using different pulse modulation techniques.

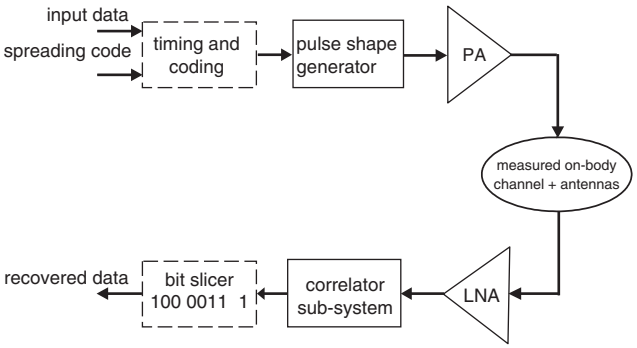

Fig. 9 *Block diagram of the UWB radio system modelled for performance analysis of potential transceivers that could be applied in body-centric networks*

Various modulation schemes are possible for UWB signalling such as pulse position modulation (PPM), amplitude shift keying (ASK), on-off keying (OOK), phase shift keying (PSK), and frequency shift keying (FSK). The performance of PPM and bi-phase modulated UWB signals in multipath environment was investigated in [9] and [10] for different data rates and under different requirements. The system model presented here applies 100 Mbit/s data rate and operates in low signal-to-noise ratio (SNR = 0) for performance analysis under measured on-body channel data.

3.2 Performance analysis

Both transmitted and received signal spectrum were examined to determine the effects of both modulation technique and channel characteristics on the system performance.

The effect of measured channel responses on received UWB pulses in both antenna cases was also analysed and investigated. Figures 10 and 11 show the transmitted and received pulses for on-body channel scenario 1 (Scenario 1, receiver placed at Rx1 on the chest with body standing still) using PPM and bi-phase modulation, respectively. The variation in time delays between the different received pulses highlights the antenna effect on the channel behaviour of the on-body links for the received pulses. More echo and noise components are introduced in the case of pulses

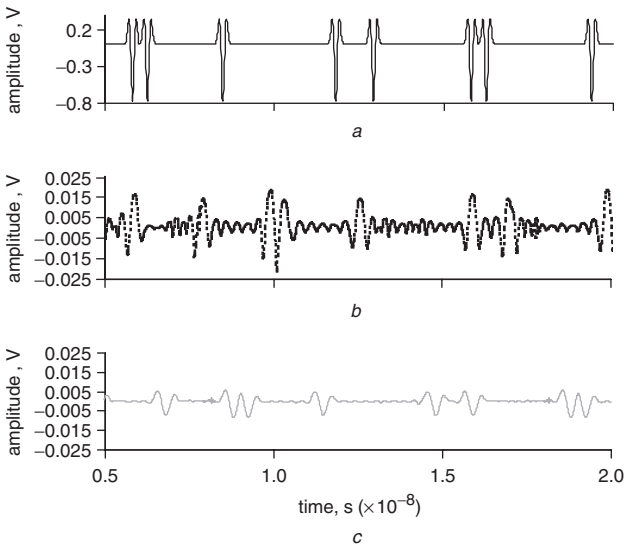

Fig. 10 *Transmitted and received UWB pulses applying PPM modulation in PICA and HSCA measurement cases (scenario 1 – Rx1 placed on the right side of the chest with body standing still)*

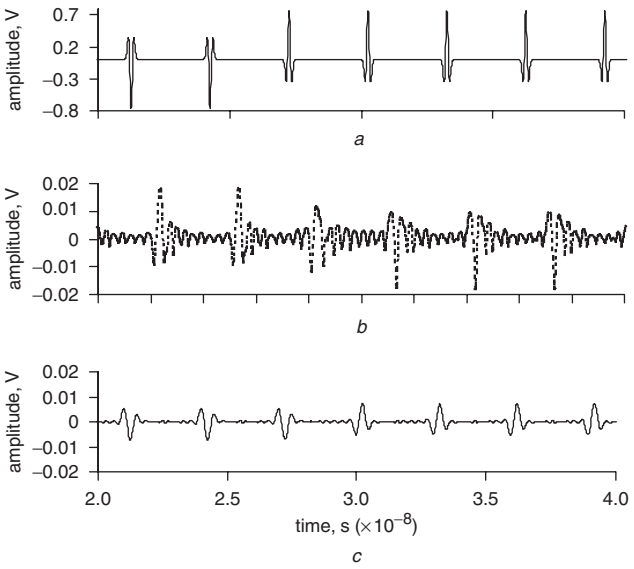

Fig. 11 *Transmitted and received UWB pulses applying bi-phase modulation in PICA and HSCA measurement cases (scenario 1 – Rx1 placed on the right side of the chest with body standing still)*

received under the PICA compared to those with the HSCA and this is due to the wider bandwidth of the HSCA antenna (as discussed earlier). However, the improved pulse shape received in HSCA case is traded off by reduction in energy received. In regards to the influence of modulation techniques on UWB pulses, bi-phase provided better robustness to multipath components in comparison to PPM cases.

As the most referred to receiver design for UWB systems, RAKE receiver is modelled to collect the pulses energy in multipath component directions. At signal-to-noise-ratio (SNR) = 0 two RAKE fingers were modelled to collect the direct path component and the second finger to collect one multipath component with average delay window of 8 ns for the investigated scenarios. The applied on-body channels are scenario 1 (Rx1 on chest body standing still), scenario 8 (Rx2 on the back with body leaning forward), scenario 14 (Rx4 on the right side of the head with head turned right) and scenario 16 (Rx5 on the left wrist with arm stretched above head). Different bit error rate (BER) values are obtained for the various investigated scenarios and for the modulation schemes applied, Fig. 12.

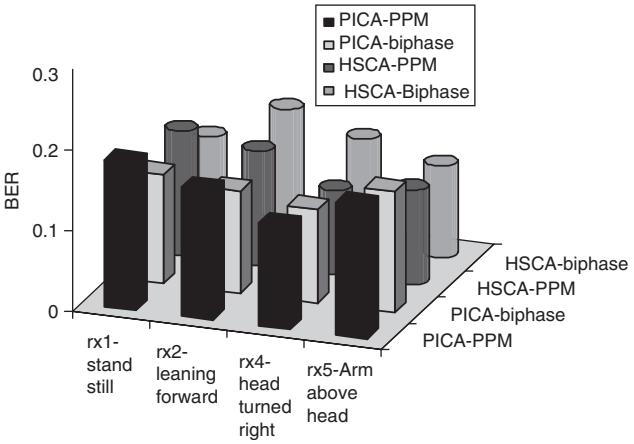

Fig. 12 *BER at specified on-body links (Rx1 with body standing still, Rx2 with body leaning forward, Rx4 with head turned right and Rx5 with arm above head) for both modulation schemes PPM and bi-phase with two rake fingers*

Differences of around 6% in BER measures are found when PPM is used in comparison to 1.5% for the bi-phase modulation system between PICA and HSCA measured channel responses. This implies that bi-phase modulation can be adopted in designing initial potential UWB transceiver designs for wireless body-centric networks since it provides better performance of UWB systems even for higher data rates, which also agree with results obtained in [10].

4 Conclusions

UWB on-body propagation channel measurements were performed in an anechoic chamber to study the deterministic characteristics of the radio channel on human body. On-body channels depend mainly on space wave and surface wave propagation; therefore the two UWB antenna types were chosen to study these propagation contributors in details and also to present vertical and planar UWB antenna characteristics. When both the transmitter and receiver are placed on the trunk (front side of the body) in the HSCA measurement stronger surface waves were available compared to the PICA case. This can be demonstrated in the variations of delay parameters between both antenna cases for different on-body channels. The channel path loss was modelled as a function of the logarithmic distance, however, it was shown that a conventional dual-slope model can be obtained to provide a path loss model as a function of distance. Received power was proven to be dependent not only on the antenna positions and distances but also on the frequency dependency of both antennas and on-body channel. Measured RMS spread delay and mean excess delay data fitted to log normal distribution that provides a tool for empirical on-body propagation modelling that can be combined with any other models representing different environments, specially with fitting results presenting slightly similar distribution coefficients for both antenna cases. The measured and analysed data were used for evaluating the performance of potential UWB transceivers that could be applied in the wireless body-centric networks. For very low transmitting power and low SNR, bi-phase modulation provided better system performance in comparison to PPM for potential UWB on-body wireless communications.

5 Acknowledgments

The authors wish to thank Mr. John Dupuy for his assistance in antenna measurement and fabrication and also for his help with propagation measurement setup. Also thanks to Miss W. Dong for her help with simulation and measurement analysis. Thankful acknowledgment goes to the reviewers for their constructive comments and suggestions.

6 References

1 Bernardhard, J., Nagel, P., Hupp, J., Strauss, W., and von der Grun, T.: 'BAN-body area network for wearable computing'. 9th Wireless World Research Forum Meeting, Zurich, Switzerland, July 2003
2 Foerster, J., Green, E., Somayazulu, S., and Leeper, D.: 'Ultra-wideband for short- or medium-range wireless communications', *Intel Technol. J.*, 2001, **5**, (2)
3 Chong, C., Kim, Y., and Lee, S.: 'UWB indoor propagation channel measurements and data analysis in various types of high-rise apartments'. Proc. IEEE Vehicular Technology Conf. (VTC2004-Fall), Los Angeles, USA, September 2004
4 Ghassemzadeh, S.S., Jana, R., Rice, C.W., Turin, W., and Tarokh, V.: 'A statistical path loss model for in-home UWB channels'. IEEE Conf. on Ultra Wideband Systems and Technologies, UWBST, Baltimore, USA, 2002, pp. 59–64
5 Alomainy, A., Owadally, A., Hao, Y., Parini, C.G., Nechayev, Y., Constantinou, C.C., and Hall, P.: 'Body-centric WLAN for future wearable computers'. First Int. Workshop on Wearable & Implantable Body Sensor Networks, London, UK Imperial College, 6–7 April 2004
6 Nechayev, Y., Hall, P., Constantinou, C.C., Hao, Y., Owadally, A., and Parini, C.G.: 'Path loss measurements of on-body propagation channels'. Proc. 2004 Int. Symp. on Antennas and Propagation, Sendai, Japan, Aug. 2004, pp. 745–748
7 Zasowski, T., Althaus, F., Stager, M., Wittneben, A., and Troster, G.: 'UWB for noninvasive wireless body area networks: channel measurements and results'. Proc. IEEE Conf. on Ultra Wideband Systems and Technologies, Reston, Virginia, Nov. 2003, pp. 285–289
8 Alomainy, A., Hao, Y., Parini, C.G., and Hall, P.S.: 'Comparison between two different antennas for UWB on-body propagation measurements', *IEEE Antennas Wirel. Propag. Lett.*, 2005, **4**, (1), pp. 31–34
9 Bastidas-Pugo, E.R., Ramirez-Mireles, F., and Munoz-Rodriguez, D.: 'Performance of UWB PPM in residential multipath environments'. IEEE 58th Vehicular Technology Conf., VTC Fall 2003, Olando, Florida, 6–9 Oct. 2003, Vol. 4, pp. 2307–2311
10 Chung, W.C., and Ha, D.S.: 'On the performance of bi-phase modulated UWB signals in a multipath channel'. IEEE Vehicular technology Conf., VTC Spring 2003, Jeju, Korea, April 2003, pp. 1654–1658
11 Saitou, A., Iwaki, T., Honjo, K., Sato, K., Koyama, T., and Watanabe, K.: 'Practical realization of self-complementary broadband antenna on low-loss resin substrate for UWB applications'. 2004 IEEE MTT-S Int. Microwave Symp. Fort Worth, Texas, June 2004
12 Suh, S.-Y., Stutzman, W.L., and Davis, W.A.: 'A new ultrawideband printed monopole antenna: the planar inverted cone antenna (PICA)', *IEEE Trans. Antennas Propag.*, 2004, **52**, (5), pp. 1361–1364
13 Rappaport, T.S.: 'Wireless communications: principles and practice' (Prentice Hall, 1999, Ch. 3, 4 and 5)